IEEE Access
Multidisciplinary ⋮ Rapid Review ⋮ Open Access Journal

Received 20 January 2025, accepted 4 February 2025, date of publication 18 February 2025, date of current version 24 February 2025.

Digital Object Identifier 10.1109/ACCESS.2025.3543183

RESEARCH ARTICLE

Machine Learning Aided Tapered Four-Port MIMO Antenna for V2X Communications With Enhanced Gain and Isolation

NAGESH KALLOLLU NARAYANASWAMY[1], (Senior Member, IEEE), YAZEED ALZAHRANI[2], (Senior Member, IEEE), KRISHNA KANTH VARMA PENMATSA[3], ASHISH PANDEY[4], AJAY KUMAR DWIVEDI[1], (Senior Member, IEEE), VIVEK SINGH[1], (Senior Member, IEEE), AND MANOJ TOLANI[5], (Senior Member, IEEE)

[1]Department of Electronics and Communication Engineering, Nagarjuna College of Engineering and Technology, Bengaluru, Karnataka 562110, India
[2]Department of Computer Engineering and Information, College of Engineering, Prince Sattam bin Abdulaziz University, Wadi ad-Dawasir 11991, Saudi Arabia
[3]Department of Electronics and Communication Engineering, Sagi Ramakrishnam Raju Engineering College, Bhimavaram, Andhra Pradesh 534204, India
[4]Department of Data Science and Engineering, Manipal University Jaipur, Jaipur, Rajasthan 303007, India
[5]Department of Information and Communication Technology, Manipal Institute of Technology, Manipal Academy of Higher Education, Manipal, Karnataka 576104, India

Corresponding author: Manoj Tolani (manoj.tolani@manipal.edu)

ABSTRACT In this communication, a 4-port Multiple-Input-Multiple-Output (MIMO) antenna is analyzed and investigated for vehicle-to-everything (V2X) communication centered at 5.9 GHz. The proposed optimized single antenna consists of a tapered radiating antenna with a defective ground structure fed with stepped impedance transmission line feed. The proposed 4-port MIMO antenna has a dimension of $96 \times 64 \times 0.8$ mm^3 printed on the FR4 substrate with a relative permittivity of 4.4 and loss tangent of 0.02. To obtain the proposed single antenna unit, parametric analysis, and evolution stages have been investigated and discussed. The impedance bandwidth of the proposed antenna is 5.66 - 6.00 GHz with a peak gain of 7.85 dB and radiation efficiency of 99%. In addition, machine learning techniques such as XG (Extreme Gradient) Boost, Random Forest, and Deep Neural Networks (DNN) were employed in the optimization process to predict and fine-tune the antenna's design parameters. The stacking ensemble method, combining these models, was used to improve the accuracy of the antenna performance prediction. By leveraging machine learning, the final design was achieved more efficiently, significantly reducing the simulation time and enabling more precise parameter tuning for optimal performance. Further, to validate the MIMO antenna characteristics, different diversity parameters have been calculated such as ECC (Envelope Correlation Coefficient), DG (Diversity Gain), CCL (Channel Capacity Loss), and TARC (Total Active Reflection Coefficient). The fabricated antenna is modeled, and measured findings are found to be in coherence with simulated findings.

INDEX TERMS MIMO, V2X, DSRC, ECC, TARC, machine learning, DNN, random forest, stacking ensemble.

I. INTRODUCTION

Dedicated short-range communications (DSRC) is a wireless technology that enables the direct exchange of data between vehicles, pedestrians, cyclists, and roadside infrastructure such as traffic signals and electronic message signs. This technology is used for vehicle-to-everything (V2X) communication and other intelligent transportation systems (ITS) data transfer [1]. DSRC utilizes channels within the approved 5.9 GHz range to provide data transfers, whether they are one-way or two-way. DSRC is built upon the IEEE 802.11p standard. Additionally, the 5.9 GHz frequency range for vehicle-to-everything connectivity was also the focus of the 3rd Generation Partnership Project (3GPP) and the 5G Automotive Association (5GAA). Table 1 shows that V2X communication is most often utilized in

The associate editor coordinating the review of this manuscript and approving it for publication was Yiming Tang.

TABLE 1. An overview of the V2X communication spectrum on a global scale.

Countries	Frequency Band (GHz)	Bandwidth (MHz)
Australia, Korea	5.855- 5.925	70
Japan	5.77- 5.850	80
China	5.905-5.925	20
Singapore, European Union	5.875- 5.925	50
United States of America	5.850- 5.925	75

the frequency region from 5.850 to 5.925 GHz, which is used all across the globe [2]. Massively multi-input multi-output (MIMO) systems have seen fast adoption in the realm of communication technology in the last few years. With MIMO technology, operators may electronically adjust the directivity of an RF signal by modulating the signal propagation phase across many antennas [3].

A further advantage of MIMO is that it may enhance data-carrying capacity without increasing bandwidth requirements via spatial multiplexing [4]. Another benefit of MIMO antenna technology is that it eliminates multipath distortion while still achieving diversity performances. Nevertheless, the data rate is reduced due to the correlation of the MIMO antenna components, which is impacted by the mutual coupling between the antenna elements [5]. Consequently, both academics and industry now give great attention to the construction of the MIMO antenna with a very low mutual coupling.

Several researchers have proposed the antenna for V2X communication. A CPW-fed dual-band (3.5 GHz (LTE (Long Term Evolution) −42 Band) and 5.9 GHz (DSRC Band) monopole antenna is presented for Vehicular to Everything (V2X) Communication [6]. In this antenna, the concept of stacked patches and slots has been used to attain the desired frequency of operation. A tri-polarized antenna with various radiation characteristics is suggested in [7]. This design has two loop radiating dipole pairs and an omnidirectional monopole antenna element for the fifth generation V2X and 5G communications, respectively. In [8] a V2X-compatible integrated multiband vertically polarized antenna using two half Vivaldi antennas and a slot antenna. For vehicle communications, it supports LTE, WiFi-2.4G, WiFi-5G, Bluetooth, and DSRC bands. In [9] authors have proposed a 3D multiband vehicle antenna designed for 5G and Vehicle to Everything (V2X) connectivity. The antenna is specifically designed to be compatible with the widely used sharkfin radome. A new planar Electronically Switched Parasitic Array Radiator (ESPAR) antenna operating at 5.9 GHz is suggested for V2X communication [10]. The antenna has pattern reconfigurability, one quasi-omni, and two directional beams, which are low-cost, simple, and small in size. A 4-port compact MIMO antenna operating in the 5.850–5.925 GHz DSRC frequency for vehicle-to-vehicle/Everything (V2V/V2X) communication is investigated in [11]. A complementary split ring resonator (CSRR) underneath each patch compacts the size. However, these proposed antennas are facing issues of mutual coupling between the antenna elements with limited gain/diversity characteristics.

The machine learning (ML) analysis performed in this research contributes significantly to optimizing the design of a single patch antenna by automating the process of parameter tuning, improving prediction accuracy for key performance metrics like $|S_{11}|$, and reducing the time required for simulation-based design iterations.

In the traditional design of a patch antenna, the parameters (such as the dimensions of the patch, ground plane, and feed line) are typically adjusted manually through a trial-and-error process or through time-consuming simulations like those conducted in HFSS (High-Frequency Structure Simulator). However, this method becomes inefficient when multiple parameters interact in complex ways. The ML analysis, particularly the stacking ensemble method combining XGBoost, Random Forest, and DNN, allows us to explore the design space more comprehensively and efficiently. By training the models on a dataset generated from HFSS simulations, the ML models learn the complex relationships between the input parameters and the output performance. This enables the models to predict the optimal parameter combination with minimal error, as demonstrated by the low MSE and high R^2 values achieved in the stacking ensemble model. This approach saves time and resources by avoiding the need to run multiple simulations manually. Instead, the ML model provides a quick and accurate estimation of how different parameter combinations will affect the antenna's performance.

Building on the discussion of machine learning's role in enhancing traditional antenna design, we explore recent breakthroughs that underscore the revolutionary effects of these technologies. Recent studies have propelled the use of machine learning in refining antenna design and performance. Sharma and colleagues employed Artificial Neural Networks (ANN) and K-Nearest Neighbors (KNN) to improve T-shaped monopole antennas, illustrating substantial performance enhancements [12]. Expanding upon these methodologies, Ranjan and his team utilized a suite of ML algorithms, including ANN, KNN, and Random Forest, to advance the design of Ultra-Wideband (UWB) printed monopole antennas, achieving notable operational improvements [13]. Additionally, Particle Swarm Optimization (PSO) and neural networks have successfully optimized dielectric resonator (DR)-based antennas, demonstrating ML's capability to manage intricate parameter interactions [14], [15].

Further integration of ML in specialized antenna applications includes a range of cutting-edge approaches. THz frequency applications have benefited from innovative uses of hybrid graphene-dielectric resonators optimized through machine learning, aligning with ensemble methods in exploring new material effects on antenna performance [16]. For sub-6 GHz 5G IoT applications, ML-enhanced MIMO antenna designs have shown efficacy. Optimization based on HFSS simulation data has led to significant performance

gains, evidenced by low MSE and high R^2 values [17]. Wu et al.'s integration of Convolutional Neural Networks (CNN) with Gaussian Process Regression (GPR) for antenna geometric optimization has proven more efficient than traditional evolutionary algorithms, complementing earlier ensemble method applications [18]. Innovative use of Random Forest with data augmentation techniques has optimized antenna designs using smaller datasets, achieving high accuracy and efficiency, thus conserving significant time and resources [19]. Lastly, Ramasamy's application of the Multiple Ant Colony Optimization (MACO) algorithm for optimizing antenna parameters in 5G communications has markedly enhanced gain and bandwidth performance [20].

These developments not only affirm the effectiveness of machine learning models in antenna design but also pave the way for further innovation, promising more advanced, efficient, and effective communication systems.

A. RESEARCH GAP AND PROPOSED APPROACH

Existing literatures [20], [21], [22], [23], [24], [25], [26], [27], and [28] has successfully leveraged single-model machine learning (ML) techniques (e.g., ANN or Random Forest) for antenna design and optimization but typically focuses on limited parameter spaces or simpler MIMO configurations. Such approaches often do not fully account for the high dimensionality and nonlinear interactions among key parameters (e.g., patch length/breadth, taper radii), nor do they systematically explore compact, multi-port antennas that maintain strong isolation without additional decoupling structures.

To address these gaps, we propose a 4-port MIMO antenna optimized via a stacked ensemble of Random Forest, XGBoost, and Deep Neural Network models. This ensemble method not only reduces the time-consuming trial-and-error often seen in conventional antenna tuning but also captures the complex parameter interactions that single-model methods may miss. Empirical results, detailed in Section III, show that the stacked ensemble achieves near-perfect R^2 for $|S_{11}|$ predictions, outperforming individual models. Consequently, while more complex than a single algorithm, it significantly enhances predictive accuracy and stability.

B. NOVELTY AND KEY CONTRIBUTIONS

Novelty and key contributions are as follows:

Stacked Ensemble Optimization: We combine Random Forest, XGBoost, and DNN, leveraging each algorithm;s unique advantages to handle the multi-parameter, nonlinear design space of a 4-port MIMO antenna at 5.9 GHz.

High Isolation without Extra Structures: Our antenna attains >25 dB isolation (up to 32 dB measured) and $\tilde{9}9\%$ radiation efficiency without using decoupling elements or additional spacing—preserving a compact form factor and distinguishing it from many existing MIMO designs.

Comprehensive MIMO Performance Evaluation: We systematically assess ECC, DG, CCL, and TARC to confirm the design's robustness for V2X and related ITS applications.

Reduced Simulation Effort: By avoiding exhaustive HFSS parameter sweeps and relying on ML-driven predictions, we streamline the optimization process, minimizing manual iterations.

C. BENEFITS OF THE STACKED ENSEMBLE

High Dimensionality & Nonlinear Interactions: Each model (RF, XGBoost, DNN) captures different aspects of the design's complexity, collectively leading to near-perfect R^2 and minimal error in $|S_{11}|$ predictions.

Robustness & Consistency: The ensemble approach mitigates overfitting and yields stable outcomes over the entire 5.5–6.5 GHz range, as evidenced by empirical comparisons (Table 3).

Comparative Empirical Evidence: Our results surpass single-model approaches, demonstrating that the ensemble's ''over-engineering'' is both practical and beneficial for complex antenna optimization.

In this paper, a novel ML optimized tapered 4-port MIMO antenna is presented for V2X communication centered at 5.9 GHz with isolation of more than 25 dB and peak gain of 7.85 dB. The proposed antenna offers isolation without requiring additional decoupling structures or distance between elements. Impedance matching is achieved by using a matched stub transmission line feed. HFSS software is used for simulated environments. The additional performance measurements of MIMO antennas, namely ECC, DG, CCL, and TARC fall within the acceptable range. The antenna's recommended frequency range of 5.83 – 6.05 GHz makes it highly suitable for V2X technology.

The subsequent sections of this work are structured as follows. Section II introduces the antenna's design and geometrical configuration, detailing both the single-element evolution and the final 4-port MIMO arrangement. It also presents the machine learning optimization framework, including dataset preparation, model architectures, and stacking ensemble methodology. Section III compares measured and simulated results, offering insights into impedance bandwidth, isolation, gain, and radiation patterns. Section IV evaluates the antenna's diversity performance through parameters such as ECC, DG, CCL, and TARC. Finally, Section V provides concluding remarks, emphasizing the key contributions and potential extensions for future work.

II. ANTENNA DESIGN AND GEOMETRICAL CONFIGURATION

The schematic layout of the proposed optimized single antenna elements, 2-port MIMO antenna, and 4-port MIMO antenna are presented in Figure 1(a), (b), and (c) respectively. The proposed single antenna unit is designed by providing tapering to a rectangular patch on both sides with a defective ground structure and energized by a stepped impedance feed line for proper impedance matching. The structure is made

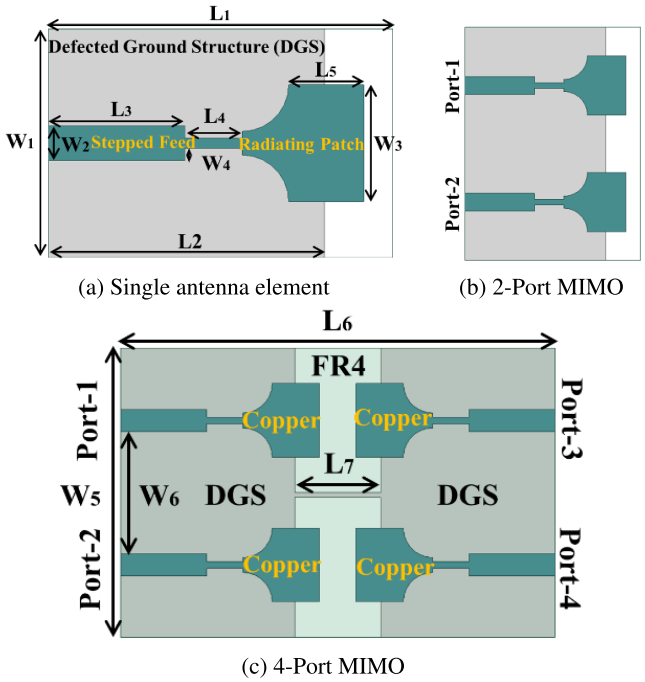

(a) Single antenna element (b) 2-Port MIMO

(c) 4-Port MIMO

FIGURE 1. Proposed antenna modules: (a) Single antenna element, (b) 2-Port MIMO Antenna, (c) 4-Port MIMO Antenna.

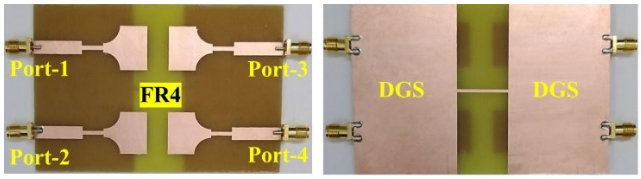

(a) (b)

FIGURE 2. Fabricated prototype of the proposed 4-Port MIMO antenna, (a) Top View (b) Back View.

up of copper printed on the FR4 epoxy substrate ($\varepsilon_r = 4.4$, $\tan\delta = 0.02$) with a thickness of 0.8 mm. The dual port MIMO antenna is designed by replicating the single antenna unit in parallel orientation (cf. figure 1(b)). Further 4-port MIMO antenna is conceived by duplicating the 2-port MIMO antenna in mirror orientation about the x-axis in front-to-front manner as shown in figure 1(c). To maintain the integrity of the MIMO antenna, the ground of all antenna elements should be connected. To fulfill this, a single conducting line of length L_7 is used to connect both the DGS planes. The dimensional specifications of the proposed module are mentioned in Table 2.

To verify the accuracy of the simulated results, a constructed model of the planned 4-port MIMO antenna was created (c.f figure 2). The fabricated prototype with measurement setup is shown in Figure 3.

A. SEQUENTIAL PROGRESSION OF SINGLE ANTENNA COMPONENTS

Figures 4(a) and 4(b) depict the advancement of an individual antenna element in antenna design and its consequent effect on return loss.

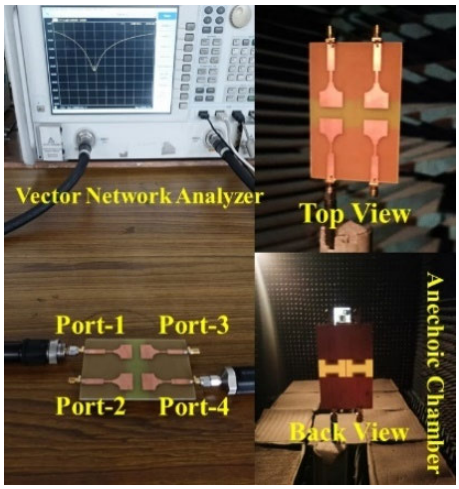

FIGURE 3. Fabricated prototype with measurement setup.

TABLE 2. Dimensional specification of the proposed modules.

Parameters	Dimensions (in mm)	Parameters	Dimensions (in mm)
L1	48	L7	19
L2	38.5	W1	32
L3	19	W2	5
L4	8	W3	16.3
L5	10.5	W4	1.67
L6	96	W5, W6	64, 27.15

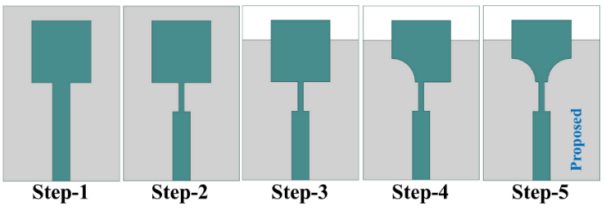

(a) Layout

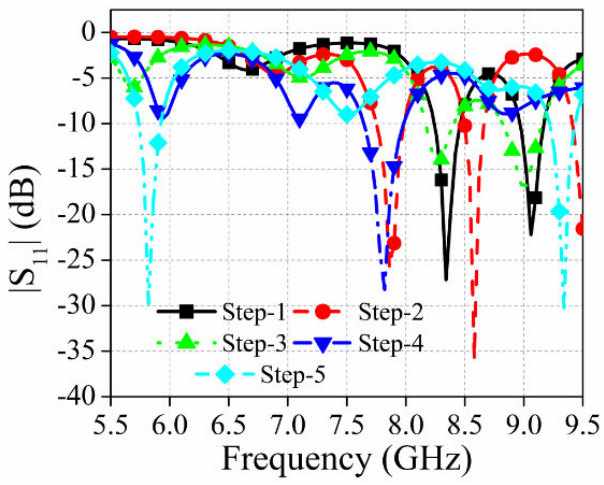

(b) Return Loss

FIGURE 4. Evolution stage of the proposed single antenna element (a) Layout (b) Return Loss.

Step 1 employs a rectangular patch antenna fed by a microstrip feed line with a fully grounded substrate. The dual resonance occurs at 8.34 GHz and 9.0 GHz, which

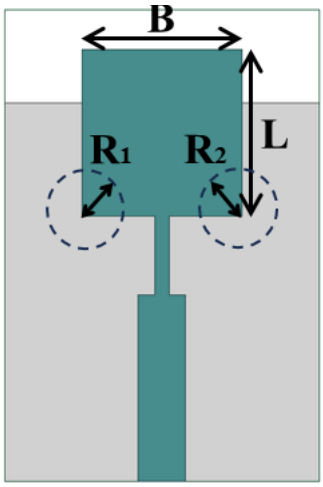

FIGURE 5. Antenna model with parameters identification for ML Optimization.

deviates from the target frequency of 5.9 GHz. In step 2, a stepped impedance feed line is used to achieve the required resonance frequency. Figure 4(b) clearly indicates that both resonant frequencies have migrated to a lower frequency region. Additionally, in step 3, the whole ground structure is transformed into a defected ground structure, leading to an expansion of the bandwidth. In step 4, the tapering on one side of the patch has been executed, leading to the suppression of the higher resonance frequency. The next phase (step 5) involves tapering on both sides of the patch to obtain the desired resonating frequency. In Step 5, the lower resonant band is centered at 5.9 GHz, which is appropriate for V2X communication. Further to optimize the structural dimensional the ML techniques has been discussed in the next section.

B. MACHINE LEARNING ANALYSIS TO ATTAIN THE OPTIMIZED DESIGN OF SINGLE ANTENNA COMPONENTS

A machine learning-based optimization approach using Extreme Gradient Boosting (XGBoost), Random Forest, Deep Neural Networks, and Stacking Ensemble Method is utilized to optimize the design of single antenna components. These algorithms are utilized for the training and testing of models with the datasets generated by HFSS.

1) DATASET GENERATION

The dataset is generated by varying the dimension of a rectangular radiating patch and the radius of tapering to a rectangular patch on both sides with a defective ground structure. The length (L) and breadth (B) of the rectangular radiating patch are varied from 15.5 mm to 17 mm and 16 mm to 17.5 mm with a linear step of 0.2 mm and 0.5 mm respectively. The radius of tapering to rectangular patch on both sides (R_1 and R_2) is varied from 5.6 mm to 7.1 mm with a linear step of 0.3 mm for both sides. It is shown in Figure 5.

The variation of L, B, R_1, and R_2 produces the 1296 combinations. The frequency sweep for the dataset generation is taken from 5.5 GHz to 6.5 GHz with 51 points. With all these varying parameters, a total of 66,096 dataset points have been generated for $|S_{11}|$. The dataset is divided into two parts i.e. training dataset comprising 80% (52,877) dataset points and the testing dataset comprising 20% (13,219) dataset points.

2) DATA PREPROCESSING

Prior to feeding the dataset into machine learning models, we performed several key preprocessing steps to ensure the integrity and consistency of the data:

a: MISSING AND ERRONEOUS DATA HANDLING

First, we inspected all records to identify any missing or anomalous values. Since our HFSS-generated dataset was large (66,096 data points), a manual inspection was not feasible; instead, we employed automated checks (e.g., identifying NaN or negative values for dimensions or frequency) to detect anomalies. Any suspicious data points—such as unintended zero or negative geometrical dimensions—were removed to maintain dataset quality.

b: FEATURE SCALING

Each of the four geometric parameters (length L, breadth B, and taper radii R_1 and R_2) was standardized using z-score normalization, defined as

$$x_{\text{scaled}} = \frac{x - \mu}{\sigma} \tag{1}$$

where x is the original value of a given feature, μ is the mean of that feature, and σ is its standard deviation. By transforming these parameters, we ensured that all features contributed equally during training, preventing any single parameter (e.g., patch length) from disproportionately influencing the learning process. We maintained the frequency dimension in its original scale to preserve its physical significance, but alternative scaling methods (e.g., min-max) could also be employed.

c: OUTLIER DETECTION

We observed that certain geometrical parameter combinations could generate spurious or physically infeasible results in HFSS (e.g., extremely poor $|S_{11}|$ values or resonance shifts far beyond 5.5–6.5 GHz). Rather than discarding the values outright, we flagged potential outliers and tested our models' sensitivity to these extremes. Our final approach retained the majority of outliers, as removing them only marginally affected the dataset size but could potentially omit valuable boundary-case information.

d: TRAIN/TESTSPLIT

After data cleaning and scaling, we split our final dataset into training and testing subsets in an 80:20 ratio, yielding 52,877 samples for training and 13,219 samples for testing. This partitioning aligns with standard practices in supervised learning, ensuring that the models are trained on a broad

subset of the parameter space while retaining a held-out portion for unbiased performance evaluation.

e: DATA SHUFFLING AND RANDOM SEEDING

We randomly shuffled the dataset before the split to eliminate any temporal or systematic ordering that might inadvertently bias training. A fixed random seed was used to facilitate reproducibility of the results. By following these preprocessing steps, we ensured that our dataset accurately reflected the antenna's design space while being optimized for machine learning algorithms. This process allowed for more reliable and efficient training, paving the way for robust model performance and accurate predictions of $|S_{11}|$ over the 5.5–6.5 GHz frequency range.

3) NETWORK ARCHITECTURE AND PROPOSED STACKING ENSEMBLE METHOD

In this section, we describe the architecture of the machine learning algorithms used in the proposed stacking Ensemble method, including XGBoost, Random Forest, and Deep Neural Networks (DNN), as well as the stacking algorithm combining these models. Additionally, we provide the mathematical equations that govern the operation of these models.

a: PROPOSED APPROACH VS. TRADITIONAL TRIAL-AND-ERROR METHODOLOGY

In traditional patch antenna design, parameter tuning is often performed through a time-consuming trial-and-error process, where design parameters are iteratively adjusted and re-simulated. In contrast, our machine learning-based approach deviates significantly by leveraging trained models that predict antenna performance with high accuracy, thereby avoiding repeated simulations. Each ML model—XGBoost, Random Forest, and DNN—contributes unique strengths to the final stacked ensemble model. XGBoost effectively captures non-linear interactions between design parameters, Random Forest provides robust predictions with reduced overfitting, and DNN models complex, non-linear relationships. By combining these models with a stacking ensemble, we create a structured and automated optimization framework that achieves high prediction accuracy without exhaustive parameter searches in HFSS. This approach markedly reduces computation time while yielding precise parameter predictions, streamlining the design process beyond traditional methods.

b: XGBoost ARCHITECTURE

XGBoost is a gradient-boosting algorithm that builds an ensemble of decision trees in a sequential manner, where each new tree aims to correct the errors of the previous ones. It uses a second-order Taylor approximation for the loss function. The objective function minimized by XGBoost consists of the loss function and a regularization term to avoid overfitting. The regularized objective function is given by:

$$\mathcal{L}(\theta) = \sum_{i=1}^{n} l(\hat{y}_i, y_i) + \sum_{k=1}^{K} \Omega(f_k) \tag{2}$$

where

$$\Omega(f_k) = \gamma T + \frac{1}{2}\lambda ||\omega||^2 \tag{3}$$

Here, $l(\hat{y}_i, y_i)$ is the loss function (commonly squared error for regression problems) and $\Omega(f_k)$ is the regularization term, where T is the number of leaves, ω is the weight of leaves, γ controls the complexity, and λ is a regularization term. The final prediction, for instance, is the sum of predictions from all trees:

$$\hat{y}_i = \sum_{k=1}^{K} f_k(x_i) \tag{4}$$

c: RANDOM FOREST ARCHITECTURE

Random Forest is an ensemble learning method that fits multiple decision trees on random subsets of the dataset and averages their predictions to improve accuracy and control overfitting. For a given dataset $D = \{(x_1, y_1), \ldots, (x_n, y_n)\}$, Random Forest grows multiple decision trees using bootstrapped datasets. Each tree is trained using a subset of the features at each split (random feature selection). The prediction for a new input x, is the average of the predictions from all the individual trees in the forest:

$$\hat{y} = \frac{1}{T}\sum_{t=1}^{T} \hat{y}_t \tag{5}$$

where T is the total number of trees, and $\hat{y}_t$ is the prediction from the t-th tree.

d: DEEP NEURAL NETWORK (MLP) ARCHITECTURE

The neural network used is a Multi-Layer Perceptron (MLP), which consists of fully connected layers with activation functions such as ReLU. The input features are processed through a series of hidden layers to predict the output (S_{11} values).

The Input Layer takes the input features (B, L, R1, R2, and frequency). The MLP has two **Hidden Layers**: The first hidden layer with 64 neurons. The second hidden layer with 32 neurons. Each layer uses an activation function (commonly ReLU, $f(x) = \max(0, x)$).

The Output Layer has a single output neuron that predicts the S_{11} value. For a **single layer** l, the transformation is:

$$z^{(l)} = W^{(l)} a^{(l-1)} + b^{(l)} \tag{6}$$

$$a^{(l)} = f(z^{(l)}) \tag{7}$$

where $W^{(l)}$ and $b^{(l)}$ are the weight matrix and bias vector for layer l. $a^{(l-1)}$ is the activation from the previous layer, and $f(z)$ is the activation function (e.g., ReLU). The loss function

for the MLP (regression problem) is typically Mean Squared Error (MSE):

$$\mathcal{L} = \frac{1}{n}\sum_{i=1}^{n}(\hat{y}_i - y_i)^2 \tag{8}$$

e: PROPOSED STACKING ENSEMBLE METHOD ARCHITECTURE

The stacking method combines the predictions of the base models (XGBoost, Random Forest, and DNN) using Ridge Regression as the meta-learner. The stacked model improves the overall prediction accuracy by leveraging the strengths of each base model. The Stacking architecture is as follows: Base Models: XGBoost, Random Forest, and DNN each predict the $|S_{11}|$ values based on the input features (B, L, R_1, R_2, Frequency). Meta-Model (Ridge Regression): The predictions of the base models are combined and passed to a Ridge Regression model for the final prediction.

The stacking model combines these predictions into a new feature vector

$$H(x) = [h_1(x), h_2(x), \ldots, h_k(x)]$$

where $h_1(x), h_2(x), \ldots, h_k(x)$ are the predictions from the base models (XGBoost, Random Forest, and DNN). Ridge Regression is then used to make the final prediction:

$$\hat{y} = \beta_0 + \sum_{j=1}^{k}\beta_j h_j(x) \tag{9}$$

where β_j are the coefficients learned by Ridge Regression. The Ridge Regression objective function is defined as:

$$\mathcal{L}(\beta) = \frac{1}{n}\sum_{i=1}^{n}(y_i - \hat{y}_i)^2 + \alpha\sum_{j=1}^{k}\beta_j^2 \tag{10}$$

where α is the regularization parameter, which controls the trade-off between fitting the data and keeping the model coefficients small.

f: STACKING PROCESS WITH GRID SEARCH

In addition to the basic stacking model architecture, hyperparameter tuning is performed using GridSearchCV to find the optimal parameters for XGBoost and Random Forest, which are then used in the stacking ensemble along with the DNN model.

g: HYPERPARAMETER TUNING

a) **XGBoost:** GridSearchCV is employed to optimize the following parameters:
   i. *n_estimators*: Number of trees in the ensemble.
   ii. *max_depth*: Maximum depth of each tree.
   iii. *learning_rate*: Step size shrinkage used to prevent overfitting.

b) **Random Forest:** The following parameters are tuned:
   i. *n_estimators*: Number of trees in the forest.
   ii. *max_depth*: Maximum depth of each tree.

TABLE 3. Performance of different ML Model.

Model		**MSE**	**RMSE**	**MAE**	**MAPE**
XGBoost	0.9816	0.8062	0.8979	0.2917	2.6451%
Random Forest	0.9882	0.5179	0.7197	0.2318	2.1692%
DNN	0.9813	0.8198	0.9054	0.4069	5.8852%
Stacking Ensemble	*0.9998*	*0.0106*	*0.1031*	*0.0417*	*0.3897%*

After hyperparameter tuning, the optimized models for XGBoost and Random Forest are selected, and their predictions are combined with those of the DNN.

The final prediction is a weighted sum of the predictions from these models, with the weights learned by Ridge Regression:

$$\hat{y} = \beta_0 + \beta_1 \cdot XGBoost(x) + \beta_2 \cdot RandomForest(x) + \beta_3 \cdot DNN(x) \tag{11}$$

h: OPTIMIZATION AND FINAL MODEL

The goal of this stacking process is to minimize the error between the stacked predictions and the true $|S_{11}|$ values. This is achieved by tuning the base models to improve their individual performances and then combining their predictions in a way that reduces the overall prediction error.

By leveraging the strengths of different models (XGBoost's ability to capture complex feature interactions, Random Forest's robustness against overfitting, and DNN's capacity for modeling non-linearities), the final stacked model provides a highly accurate prediction of the $|S_{11}|$ values, improving the performance over any single model.

4) RESULTS AND ANALYSIS THROUGH ML

In this section, we present and analyse the results obtained from our machine learning-based optimization of the proposed antenna design, focusing on predicting the $|S_{11}|$ parameter. We compare the performance of individual machine learning models (XGBoost, Random Forest, Deep Neural Networks) as well as the proposed stacking ensemble method, which combines these models with a Ridge regression meta-learner. We also highlight the optimal combination of antenna parameters (B, L, R_1, R_2) derived from the grid search process and evaluate the accuracy of the $|S_{11}|$ predictions against the actual values obtained from HFSS simulations.

a: PERFORMANCE OF INDIVIDUAL MODELS

Three individual machine learning models were trained and tested: XGBoost, Random Forest, and a Deep Neural Network (DNN). The dataset was split into 80% training and 20% testing data. The evaluation of each model was based on several performance metrics, including Mean Squared Error (MSE), Root Mean Squared Error (RMSE), Mean Absolute Error (MAE), and R-squared (R^2). The performance of each model is summarized in Table 3:

The stacking Ensemble model outperformed the other models, achieving an exceptionally high R^2 value of 0.9998 and a very low MSE of 0.0106, indicating that the predictions closely matched the actual $|S_{11}|$ values across the entire frequency range. While both XGBoost and DNN

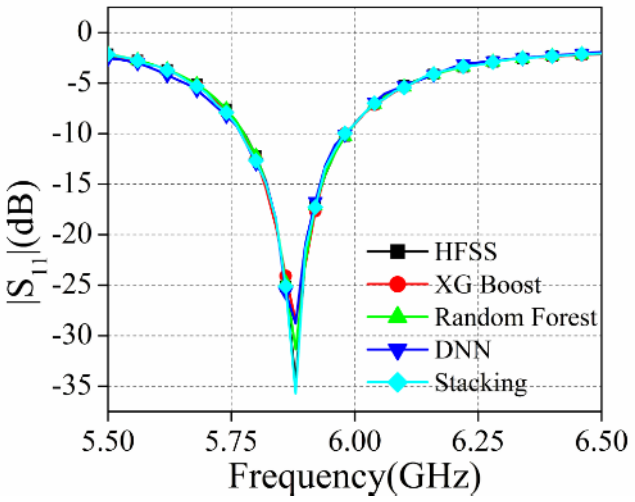

FIGURE 6. Comparison of all ML models and HFSS values of $|S_{11}|$.

performed reasonably well, they showed slightly higher errors, especially in predicting extreme $|S_{11}|$ values.

The Random Forest also demonstrated competitive performance, with an R^2 value of 0.9882 and an MSE of 0.5179, which improved upon the individual performance of XGBoost and DNN.

b: PREDICTION COMPARISON ACROSS FREQUENCY RANGE

The comparison between HFSS simulations and the predictions from each model across the frequency range (5.5 GHz to 6.5 GHz) is illustrated in Figure 6. As seen, all models closely follow the HFSS $|S_{11}|$ curve, with the stacking ensemble model and Random Forest providing the closest fit.

The Stacking Ensemble model shows an almost perfect alignment with the HFSS data, particularly near the resonance point (around 5.9 GHz), where the $|S_{11}|$ values dip. The Random Forest model also performs well across the frequency range, slightly deviating from HFSS values at higher frequencies, while XGBoost and DNN show noticeable deviations in the extreme frequency regions.

c: OPTIMAL ANTENNA PARAMETERS

Using the stacking model, we performed a grid search to identify the optimal combination of antenna parameters (B, L, R_1, R_2) that minimizes the total error across the entire frequency range. The optimal combination was found to be: B = 17.0 mm, L = 16.3 mm, R_1 = 6.5 mm, R_2 = 6.5 mm. This configuration resulted in the minimum total error of 0.1759, which indicates a highly accurate prediction of the $|S_{11}|$ values using the machine learning models. The optimal combination was saved for further validation and use in practical applications of the antenna design.

d: ANALYSIS OF RESULTS

The results demonstrate the effectiveness of machine learning in optimizing antenna design parameters. The stacking model, after optimization, proved to be a powerful tool for combining the predictions of XGBoost, Random Forest, and DNN, achieving high accuracy with minimal error. The use of Ridge regression as the meta-learner significantly improved the performance of the stacking model, particularly in reducing MSE and MAE. Among the individual models, Random Forest consistently performed the best, likely due to its ability to capture complex relationships and interactions between the input features (B, L, R_1, R_2, Frequency). However, combining multiple models in the stacking approach leveraged the strengths of each model, leading to an overall improvement in prediction accuracy.

The identification of the optimal antenna parameters (B, L, R_1, R_2) highlights the practicality of using machine learning for design optimization in high-frequency antenna systems. This approach reduces the need for extensive manual tuning and offers a more efficient way to achieve the desired performance metrics, such as high isolation and low $|S_{11}|$ values. The proposed stacking ensemble method, along with the individual machine learning models, demonstrated exceptional accuracy in predicting the $|S_{11}|$ values for the MIMO antenna design. The optimization of hyperparameters and the use of Ridge regression as a meta-learner contributed to the success of the stacking model, making it a valuable tool for antenna designers looking to improve performance while reducing manual effort. The optimal combination of antenna parameters found through this process offers a promising design for V2X communication systems.

C. 4-PORT MIMO ANTENNA

The $|S_{11}|$ plot for all four ports and mutual coupling plots between all the ports have been shown in Figures 7(a) and (b) respectively. From the perusal of Figure 7(a) it is observed that the reflection coefficient graph is similar for all the ports resonating at 5.9 GHz with impedance bandwidth of 5.83 - 6.05 GHz. The highest isolation of more than 27 dB is observed between the port pairs (Port-1/Port-2) and (Port-3/Port-4), while for port pairs (Port-1/Port-4) and (Port-2/Port-3) the isolation of more than 19 dB and comparatively less isolation is observed between the port pairs (Port-1/Port-3) and (Port-2/Port-4) which is more than 16 dB. To simplify the construction, no further decoupling mechanism is included since there is a significant amount of overall isolation between the ports.

D. ELECTRIC FIELD DISTRIBUTION

The electric field distribution plot of the 4-port MIMO antenna is presented in Figure 8. These plots are obtained by energizing one port by keeping the other port matched and terminated by 50 Ω. From the perusal of Figure 8 it is observed that when port-1 is energized, then most of the electric field is confined to the port-1 antenna structure and a small effect can be observed in port-3 which is close to port-1 (front-to-front orientation). While other ports (port-2 and port-4) are less correlated with port-1. The same behavior can be observed when other ports are energized subsequently.

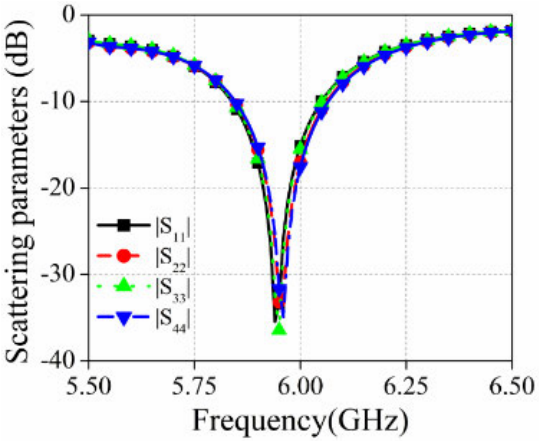

(a) $|S_{11}|$ (dB)

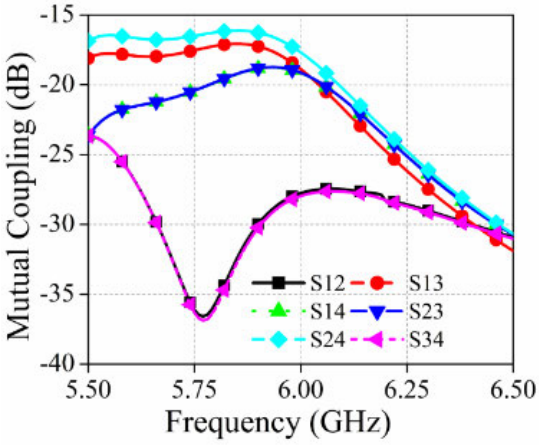

(b) Mutual Coupling

FIGURE 7. Scattering parameters of the Proposed 4-port MIMO antenna, (a) $|S_{11}|$ (dB), (b) Mutual Coupling.

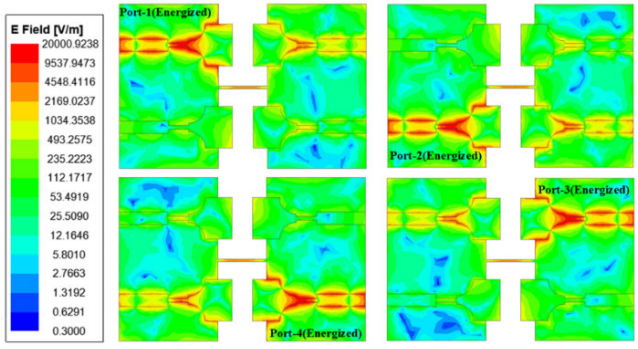

FIGURE 8. Electric field distribution plots of the proposed MIMO antenna.

III. MEASURED/SIMULATED FINDINGS

This section of the writing concentrates on three crucial elements: (i) Verification of simulated outcomes by comparison with measured findings (ii) To compute the diversity metrics, (iii) The Four-port MIMO antenna that is being suggested is being compared to existing research in the field. To validate the simulated performance, the antenna prototype, shown in Figure 3, is assessed using the E5071C Keysight-based VNA (Vector Network Analyzer). The graphs in

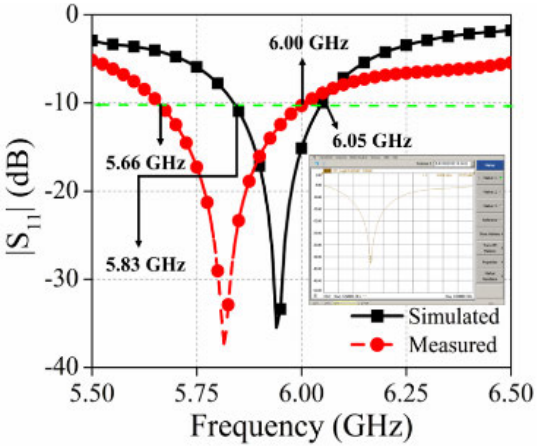

(a) $|S_{11}|$

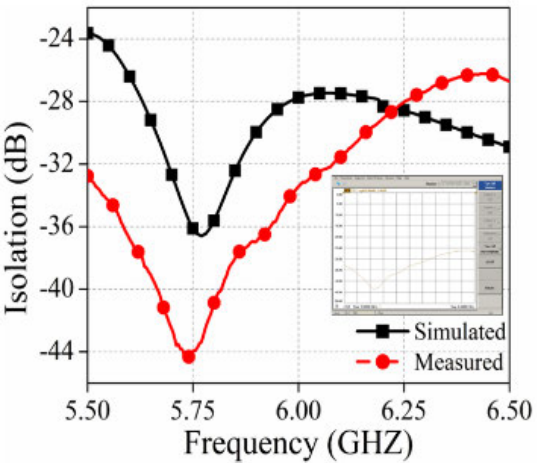

(b) $|S_{12}|$

FIGURE 9. Simulated and measured, (a) $|S_{11}|$ (b) $|S_{12}|$ for the proposed module.

Figures 9(a) and 9(b) display the simulated and measured findings in the $|S_{11}|$ and $|S_{12}|$ values of the proposed antenna radiator. From the perusal of Figure 9(a), it is observed that the simulated impedance bandwidth is 5.83 GHz to 6.05 GHz (220 MHz) while the measured bandwidth is 5.66 GHz to 6.00 GHz (340 MHz). The simulated and measured isolation plot for $|S_{12}|$ is presented in Figure 9(b) which represents that the simulated value is more than 27 dB and the measured value is more than 32 dB for the aforementioned impedance bandwidth. Small discrepancies are found between simulated and measured findings due to fabrication tolerance and human error.

The simulated/measured Gain and simulated radiation efficiency plot for the proposed antenna module is shown in Figure 10. The figure reveals two conclusions: (i) as the frequency rises, the gain also increases due to the larger effective aperture of the radiator concerning the wavelength; (ii) the radiation efficiency remains over 99% throughout the full impedance bandwidth.

The Two-dimensional radiation patterns (Co and Cross-polarization) in the E-plane and H-plane are shown in Figure 11 for the suggested antenna. In both planes,

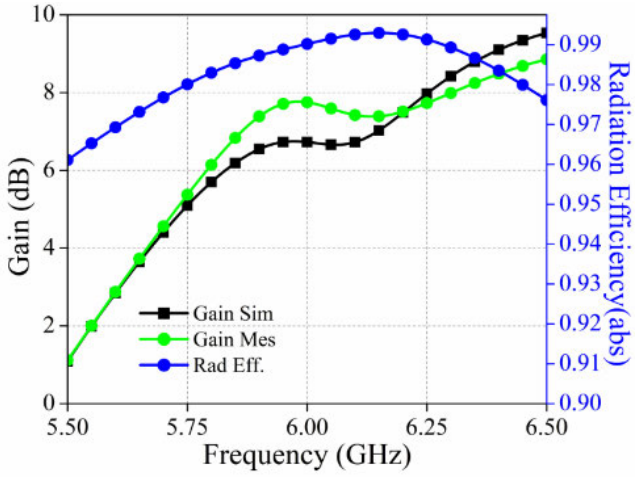

FIGURE 10. Simulated/Measured Gain and Simulated radiation efficiency.

the co-polarization level outperforms the cross-polarization level by 15-20 dB. Omnidirectional radiation behavior was observed for the proposed radiator.

IV. DIVERSITY PERFORMANCE

A. ENVELOPE CORRELATION COEFFICIENT (ECC) AND DIVERSITY GAIN (DG)

When it comes to performance metrics like polarization and radiation patterns, the ECC determines how autonomous MIMO components are effectively calculated. The Envelope Correlation Coefficient (ECC), denoted as ρ_{eij}, of the proposed Multiple-Input Multiple-Output (MIMO) antenna system, is calculated using the S-parameters and far-field radiation. The calculation is performed using equation (12) for the S-parameters and equation (13) for the far-field radiation, as mentioned [21]].

$$\rho_{eij} = \frac{|S_{ii}S_{ij}^* + S_{ji}S_{jj}^*|}{(1-|S_{ii}|^2-|S_{ji}|^2)(1-|S_{jj}|^2-|S_{jj}|^2)} \tag{12}$$

$$\rho_{eij} = \frac{\left|\int_\Omega 4\pi[\vec{R}_i(\theta,\varphi)\times\vec{R}_j^*(\theta,\varphi)]d\Omega\right|^2}{\int_\Omega 4\pi R_i(\theta,\varphi)^2 d\Omega \int_\Omega 4\pi R_j(\theta,\varphi)^2 d\Omega} \tag{13}$$

The reflection coefficient is denoted as S_{ii}, whereas the transmission coefficient is denoted as S_{ij}. The radiation values of the i-th and j-th antennas in three dimensions are denoted as $\vec{R}_i(\theta,\varphi)$ and $\vec{R}_j(\theta,\varphi)$ accordingly. The solid angle is represented by Ω. If the radiation efficiency of the proposed antenna is more than 90% then calculation of ECC by scattering parameters can be considered an effective method. The value of ECC for the proposed 4-port MIMO antenna is shown in Figure 12 (a) which is less than 0.001 for the operating impedance bandwidth.

Another crucial statistic is the diversity gain (DG), which quantifies the impact of the MIMO antenna's diversity scheme on the emitted power. The DG (Directivity Gain) for the proposed MIMO antenna is determined by calculating the value of S-parameters using Equation 14-22 [22] and is

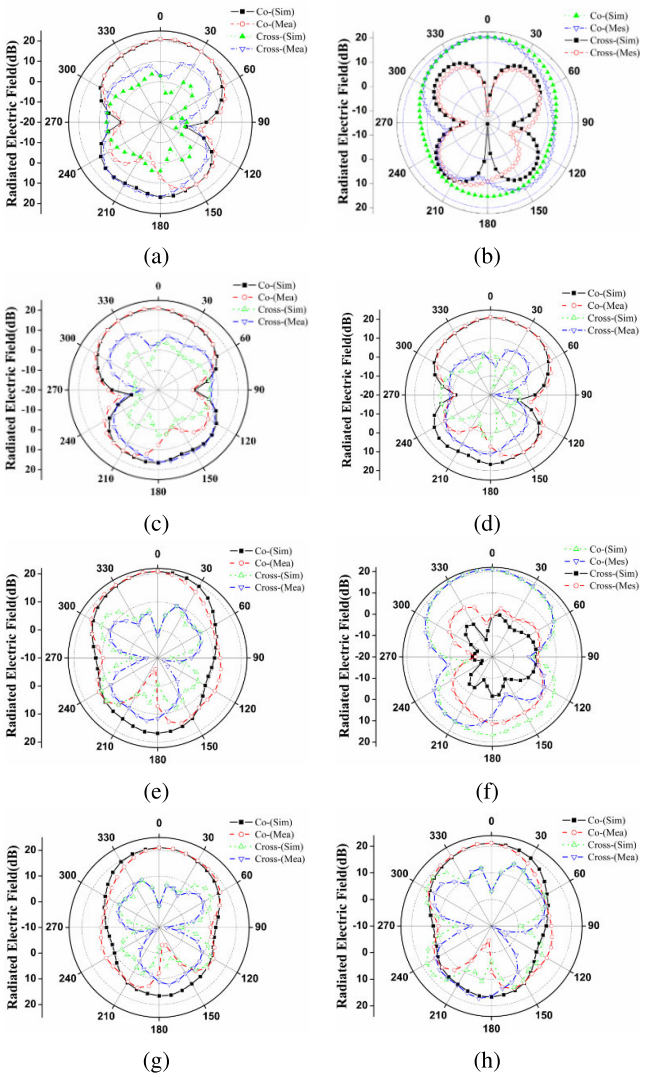

FIGURE 11. Two-Dimensional radiation patterns (a) Port-1 E-Plane, (b) Port-1 H-Plane, (c) Port-2 E-Plane, (d) Port-2 H-Plane, (e) Port-3 E-Plane, (f) Port-3 H-Plane, (g) Port-4 E-Plane, (h) Port-4 H-Plane.

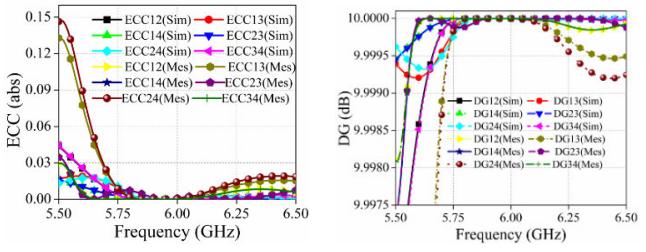

(a) ECG (b) DG

FIGURE 12. Diversity characteristics of the MIMO antenna (a) ECC, (b) DG.

shown in Fig. 12(b).

$$DG = 10\log\left(\sqrt{1-|\rho_{eij}|^2}\right) \tag{14}$$

The suggested MIMO antenna has a diversity gain above 9.99 dB for all antenna components, a number that closely approximates the optimum value.

TABLE 4. Comparative analysis of the performance of the Mimo antenna suggested in this study with that of earlier research.

References	*No. of Ports*	*Center Frequency (GHz)*	*Maximum Gain (dB)/ Peak Radiation Efficiency (%)*	*Isolation (dB)*	*ECC (abs)*
[2]	4	5.9	7.68/94	> 34	< 0.001
[25]	4	3.59	8.72/92	> 32	< 0.001
[26]	4	4.15	7.5/80	> 15	< 0.03
[27]	4	4.15	6.8/84	> 13	< 0.05
[28]	4	7.9	6.94/NG	> 21	< 0.001
Proposed Work	*4*	*5.9*	*7.85/99*	*>32*	*<0.001*

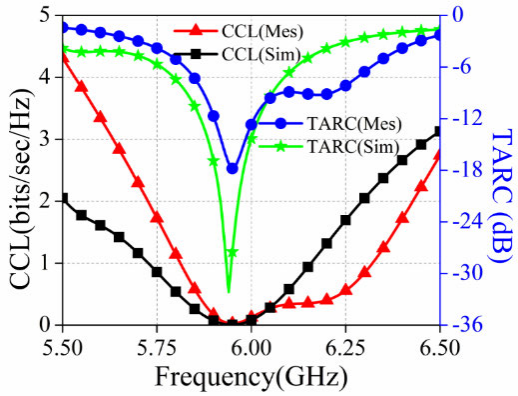

FIGURE 13. Diversity characteristics of the MIMO antenna CCL and TARC.

B. CHANNEL CAPACITY LOSS (CCL) AND TOTAL ACTIVE REFLECTIVE COEFFICIENT (TARC)

Channel Capacity Loss is a quantitative measure that predicts the highest level of channel loss that permits a message to be carried effectively over a communication channel. To provide dependable communication, the CCL mustn't surpass 0.4 bits per second per Hertz. The formula for determining the CCL may be found in equation (15) [23].

$$CCL = -\log_2 \det |N_{ant}| \tag{15}$$

$$N_{ant} = \begin{bmatrix} p_{11} & p_{12} & p_{13} & p_{14} \\ p_{21} & p_{22} & p_{23} & p_{24} \\ p_{31} & p_{32} & p_{33} & p_{34} \\ p_{41} & p_{42} & p_{43} & p_{44} \end{bmatrix} \tag{16}$$

Figure 13 displays the simulated and measured CCL value for the proposed frequency bandwidth which is less than 0.20 bits/sec/Hz. Under MIMO limitations, the reflection coefficient that is obtained from scattering characteristics is inadequate to forecast antenna performance. An essential metric for comprehending the radiation effect of a single antenna element on the operation of other antenna components is the total active reflection coefficient (TARC). TARC refers to the return loss of the whole MIMO antenna array.

TARC may be defined mathematically as the ratio between the square root of the total reflected power and the square root of the total incident power. The simulated and measured TARC value is less than -10 dB across the whole operational bandwidth (5.83-6.05 GHz) as seen in Figure 13 and can be calculated by equation (16). The TARC for the N-Port antenna may be defined as [24].

$$TARC = \frac{\sum_i^N (b_i^2)}{\sum_i^N (a_i^2)} \tag{17}$$

The incident signal is represented by "a" while the reflected signal is represented by "b".

A comparison between the proposed 4-port MIMO antenna and the other 4-port MIMO antenna is presented for different wireless communications. The comparison has been made in terms of gain/radiation efficiency, isolation, and diversity parameters. The comparative table shows that the performance parameters in terms of radiation characteristics (gain/radiation efficiency) isolation and ECC are optimum compared to the previously reported 4-port MIMO antennas.

V. CONCLUSION

A novel design of a 4-port MIMO antenna for V2X communication is conceived, analyzed, and investigated in this research article. The designed module of size 96 × 64 × 0.8 mm3 is resonating at 5.9 GHz with the measured bandwidth of 5.66 – 6.00 GHz (340 MHz) which makes it a suitable contender for V2X communication. The machine learning analysis by leveraging models like XGBoost, Random Forest, and Deep Neural Networks, and combining them through a stacking ensemble, predict critical performance metrics like S_{11} with high accuracy. This approach reduces the dependency on extensive HFSS simulations, accelerates the design process, and ensures that the optimal design configuration is achieved. Diversity metrics in terms of ECC, DG, CCL, and TARC are also calculated and found to be in coherence with simulated outcomes. The comparative investigation of the proposed module with other printed antennas for wireless communication also signifies the novelty of the module.

REFERENCES

[1] S. Gyawali, S. Xu, Y. Qian, and R. Q. Hu, "Challenges and solutions for cellular based V2X communications," *IEEE Commun. Surveys Tuts.*, vol. 23, no. 1, pp. 222–255, 1st Quart., 2021, doi: 10.1109/COMST.2020.3029723.

[2] Md. A. Sufian, N. Hussain, A. Abbas, J. Lee, S. G. Park, and N. Kim, "Mutual coupling reduction of a circularly polarized MIMO antenna using parasitic elements and DGS for V2X communications," *IEEE Access*, vol. 10, pp. 56388–56400, 2022, doi: 10.1109/ACCESS.2022.3177886.

[3] A. K. Dwivedi, N. K. Narayanaswamy, K. K. V. Penmatsa, S. K. Singh, A. Sharma, and V. Singh, "Circularly polarized printed dual port MIMO antenna with polarization diversity optimized by machine learning approach for 5G NR n77/n78 frequency band applications," *Sci. Rep.*, vol. 13, no. 1, p. 13994, Aug. 2023, doi: 10.1038/s41598-023-41302-2.

[4] A. K. Singh, A. K. Dwivedi, C. Choubey, and V. Singh, "Design and investigation of compact backed mirror two-port MIMO antenna for n257 (30 GHz) 5G spectrum," *J. Infr., Millim., Terahertz Waves*, vol. 45, nos. 5–6, pp. 538–555, Jun. 2024, doi: 10.1007/s10762-024-00982-1.

[5] X. Chen, S. Zhang, and Q. Li, "A review of mutual coupling in MIMO systems," *IEEE Access*, vol. 6, pp. 24706–24719, 2018, doi: 10.1109/ACCESS.2018.2830653.

[6] K. G. S. Narayan, J. A. Baskaradas, and D. R. Kumar, "Design of a CPW-fed compact MIMO antenna for next generation vehicle to everything (V2X) communication," *Wireless Pers. Commun.*, vol. 120, no. 3, pp. 2179–2200, Oct. 2021, doi: 10.1007/s11277-021-08922-1.

[7] B. Feng, J. Chen, S. Yin, C.-Y.-D. Sim, and Z. Zhao, "A tri-polarized antenna with diverse radiation characteristics for 5G and V2X communications," *IEEE Trans. Veh. Technol.*, vol. 69, no. 9, pp. 10115–10126, Sep. 2020, doi: 10.1109/TVT.2020.3005959.

[8] Y. Hua, L. Huang, and Y. Lu, "A compact 3-Port multiband antenna for V2X communication," in *Proc. IEEE Int. Symp. Antennas Propag. USNC/URSI Nat. Radio Sci. Meeting*, Jul. 2017, pp. 639–640, doi: 10.1109/APUSNCURSINRSM.2017.8072362.

[9] R. F. Corradi, S. Lenzini, F. Melli, A. Notari, and L. Vincetti, "3D automotive antenna for 5G and V2X communications," in *Proc. 34th Gen. Assem. Sci. Symp. Int. Union Radio Sci. (URSI GASS)*, Aug. 2021, pp. 1–4, doi: 10.23919/URSIGASS51995.2021.9560634.

[10] D. K. Rongas, A. S. Paraskevopoulos, L. D. Marantis, and A. G. Kanatas, "An integrated shark-fin reconfigurable antenna for V2X communications," *Prog. Electromagn. Res. C*, vol. 100, pp. 1–16, 2020, doi: 10.2528/pierc19112005.

[11] D. Gangwar and A. Patnaik, "A compact CSRR loaded 4-Port MIMO antenna for V2X communication," in *Proc. Int. Conf. Electr., Electron., Commun. Comput. (ELEXCOM)*, Aug. 2023, pp. 1–5, doi: 10.1109/elexcom58812.2023.10370545.

[12] Y. Sharma, H. H. Zhang, and H. Xin, "Machine learning techniques for optimizing design of double T-shaped monopole antenna," *IEEE Trans. Antennas Propag.*, vol. 68, no. 7, pp. 5658–5663, Jul. 2020, doi: 10.1109/TAP.2020.2966051.

[13] P. Ranjan, A. Maurya, H. Gupta, S. Yadav, and A. Sharma, "Ultra-wideband cpw fed band-notched monopole antenna optimization using machine learning," *Prog. Electromagn. Res. M*, vol. 108, pp. 27–38, 2022, doi: 10.2528/pierm21122802.

[14] C. Hu, J. P. Zhao, and J. Xu, "Optimization of dielectric resonator antenna based on machine learning and PSO methods," in *Proc. Int. Conf. Microw. Millim. Wave Technol. (ICMMT)*, Sep. 2020, pp. 1–3, doi: 10.1109/ICMMT49418.2020.9386611.

[15] N. Sehrawat, B. K. Kanaujia, and A. Agarwal, "Material perturbation in rectangular dielectric resonator antenna using neural network," in *Proc. Int. Conf. Ind. Electron. Res. Appl. (ICIERA)*, Dec. 2021, pp. 1–4, doi: 10.1109/ICIERA53202.2021.9726731.

[16] R. K. Mongia and P. Bhartia, "Dielectric resonator antennas—A review and general design relations for resonant frequency and bandwidth," *Int. J. Microw. Millim.-Wave Comput.-Aided Eng.*, vol. 4, no. 3, pp. 230–247, Jul. 1994, doi: 10.1002/mmce.4570040304.

[17] P. Ranjan, A. Krishnan, A. K. Dwivedi, S. K. Singh, and A. Sharma, "Design and optimization of MIMO dielectric resonator antenna using machine learning for sub-6 GHz based on 5G IoT applications," *Arabian J. Sci. Eng.*, vol. 48, no. 11, pp. 14671–14679, Nov. 2023, doi: 10.1007/s13369-023-07830-9.

[18] Q. Wu, W. Chen, C. Yu, H. Wang, and W. Hong, "Machine-learning-assisted optimization for antenna geometry design," *IEEE Trans. Antennas Propag.*, vol. 72, no. 3, pp. 2083–2095, Mar. 2024, doi: 10.1109/TAP.2023.3346493.

[19] J. Zhang, J. Xu, Q. Chen, and H. Li, "Machine learning assisted antenna optimization with data augmentation," *IEEE Antennas Wireless Propag. Lett.*, vol. 22, no. 8, pp. 1932–1936, Aug. 2023, doi: 10.1109/LAWP.2023.3269811.

[20] R. Ramasamy, V. Rajavel, D. Ghoshal, R. Jain, R. Nanmaran, and S. Srimathi, "An intelligent antenna optimization using machine learning algorithm for 5G applications," in *Proc. Int. Conf. Adv. Data-Driven Comput. Intell. Syst.*, 2024, pp. 325–336, doi: 10.1007/978-981-99-9518-9_24.

[21] M. S. Sharawi, "Printed multi-band MIMO antenna systems and their performance metrics [Wireless Corner]," *IEEE Antennas Propag. Mag.*, vol. 55, no. 5, pp. 218–232, Oct. 2013, doi: 10.1109/MAP.2013.6735522.

[22] A. K. Dwivedi, A. Sharma, A. K. Singh, and V. Singh, "Metamaterial inspired dielectric resonator MIMO antenna for isolation enhancement and linear to circular polarization of waves," *Measurement*, vol. 182, Sep. 2021, Art. no. 109681, doi: 10.1016/j.measurement.2021.109681.

[23] H. H. Tran and N. Nguyen-Trong, "Performance enhancement of MIMO patch antenna using parasitic elements," *IEEE Access*, vol. 9, pp. 30011–30016, 2021, doi: 10.1109/ACCESS.2021.3058340.

[24] A. K. Dwivedi, A. Sharma, A. K. Singh, and V. Singh, "Circularly polarized quad-port MIMO dielectric resonator antenna with beam tilting feature for vehicular communication," *IETE Tech. Rev.*, vol. 39, no. 2, pp. 389–401, Jan. 2021, doi: 10.1080/02564602.2020.1862714.

[25] Md. A. Sufian, N. Hussain, H. Askari, S. G. Park, K. S. Shin, and N. Kim, "Isolation enhancement of a metasurface-based MIMO antenna using slots and shorting pins," *IEEE Access*, vol. 9, pp. 73533–73543, 2021, doi: 10.1109/ACCESS.2021.3079965.

[26] K.-L. Wong, X.-Q. Ye, and W.-Y. Li, "Wideband four-port single-patch antenna based on the quasi-$TM_{1/2,1/2}$ mode for 5G MIMO access-point application," *IEEE Access*, vol. 10, pp. 9232–9240, 2022, doi: 10.1109/ACCESS.2022.3144231.

[27] K.-L. Wong, J.-Z. Chen, and W.-Y. Li, "Four-port wideband annular-ring patch antenna generating four decoupled waves for 5G multi-input-multi-output access points," *IEEE Trans. Antennas Propag.*, vol. 69, no. 5, pp. 2946–2951, May 2021, doi: 10.1109/TAP.2020.3025237.

[28] S.-H. Kim and J.-Y. Chung, "Analysis of the envelope correlation coefficient of MIMO antennas connected with suspended lines," *J. Electromagn. Eng. Sci.*, vol. 20, no. 2, pp. 83–90, Apr. 2020, doi: 10.26866/jees.2020.20.2.83.

NAGESH KALLOLLU NARAYANASWAMY (Senior Member, IEEE) received the Ph.D. degree from Jawaharlal Nehru Technological University Anantapur (JNTUA), Anantapur, Andhra Pradesh, India, in 2016. He is currently a Professor and the Head of the Department of Electronics and Communication Engineering, Nagarjuna College of Engineering and Technology, Bengaluru, India. He has authored or co-authored more than 45 research papers in international journal/conference proceedings. He is a Life Member of IETE, and various other societies, such as the Antennas Wave and Propagation Society.

YAZEED ALZAHRANI (Senior Member, IEEE) received the B.Tech. degree in computer information systems from Al-Baha University, in 2010, the M.Tech. degree from DePaul University, in 2016, and the Ph.D. degree in computer and software engineering from the University of Wollongong, in 2023. He is currently an Assistant Professor with the Department of Computer Engineering, College of Engineering, Prince Sattam bin Abdulaziz University, Wadi ad-Dawasir branch, Saudi Arabia. He specializes in emerging technologies, including AI/ML, IoT/IIoT/IoMT, UAVs, computer vision, requirements engineering, and digital twins.

KRISHNA KANTH VARMA PENMATSA received the Ph.D. degree in electronics and communication engineering from VTU Belagavi, India, in 2023. He is currently an Assistant Professor with the Department of Electronics and Communication Engineering, Sagi Ramakrishnam Raju Engineering College, Bhimavaram, India. He has more than 15 years of teaching experience. His research interests include MIMO antenna design, the IoT applications, and machine learning. He has publications in several SCI and Scopus-indexed journals and has more than 20 Scopus-indexed publications, while also serving as a reviewer for reputed journals. He is a fellow of IETE and a Life Member of IE.

ASHISH PANDEY received the M.Tech. degree in computer science and engineering from KNIT Sultanpur With more than 16 years of experience, he specializes in machine learning, cryptography, and antenna optimization. He is currently pursuing the Ph.D. degree in computer science and engineering with NIT Meghalaya. He is an Assistant Professor with the Department of Data Science and Engineering, Manipal University Jaipur, India. His research focuses on MIMO antenna design and 5G/mm-wave technologies. He has published extensively in SCI and Scopus-indexed journals. He is a member of the Cryptology Research Society of India and ACM, while also serving as a reviewer for key journals.

AJAY KUMAR DWIVEDI (Senior Member, IEEE) received the B.Tech. degree in electronics and communication engineering from Uttar Pradesh Technical University, Lucknow, India, in 2010, the M.Tech. degree in wireless communication engineering from the Sam Higginbottom University of Agriculture, Technology and Sciences, Deemed University, Allahabad, India, in 2015, and the Ph.D. degree from the Department of Electronics and Communication Engineering, Indian Institute of Information Technology Allahabad, Prayagraj, Uttar Pradesh, India, in 2021. He is currently the Dean of Research and Development and an Associate Professor with the Department of Electronics and Communication Engineering, Nagarjuna College of Engineering and Technology, Bengaluru, Karnataka, India. He has 14 years of teaching and research experience. He has authored or co-authored more than 75 research papers in international/national journal/conference proceedings. His research interests include RF and microwave, dielectric resonator antenna, MIMO DRA, and metamaterial-based dielectric resonator antenna. He is a Life Member of IETE, ISTE, IAENG, and various other societies, such as the IEEE Antennas and Propagation Society, and the IEEE Microwave Theory and Technology Society. He is a Reviewer of many international/national journal/conference proceedings, such as IEEE TRANSACTIONS ON VEHICULAR TECHNOLOGY, IEEE SENSORS LETTERS, *Wireless Personal Communications*, *International Journal of Circuit Theory and Applications*, *Computer Networks*, *Computers and Electrical Engineering*, *Journal of Infrared, Millimeter and Terahertz Waves and Waves in Random and Complex Media*, *Journal of Electronic Materials*, *International Journal of Communication Systems*, IEEE ACCESS, *Applied Optics*, *Hindawi*, *Measurement Science and Technology*, IEEE INTERNET OF THINGS JOURNAL.

VIVEK SINGH (Senior Member, IEEE) received the B.Tech. degree in electronics and communication engineering from Uttar Pradesh Technical University, Lucknow, India, in 2009, and the M.Tech. and Ph.D. degrees from the Department of Electronics and Communication Engineering, the University of Allahabad (Central University), Uttar Pradesh, India, in 2012 and 2019, respectively. He is currently an Associate Professor with the Department of Electronics and Communication Engineering, Nagarjuna College of Engineering and Technology, Bengaluru, India. He has been in the academic and research fields for more than 12 years and has guided many UG, PG, and Ph.D. students. He has authored or co-authored more than 45 research papers in international journal/conference proceedings. His research interests include printed antennas, dielectric resonator antennas, MIMO antennas, metamaterial-based antennas, and RF Communication systems. He is a reviewer of many Web of Science/Scopus-indexed journals and international conference proceedings. He is a Fellow Member of IETE, and various other societies, such as the Antennas Wave and Propagation Society.

MANOJ TOLANI (Senior Member, IEEE) received the B.Tech. degree from the IIMT Engineering College, Meerut, India, in 2010, the M.Tech. degree from the Department of Electronics and Communication Engineering, Madan Mohan Malviya University of Technology, Gorakhpur, India, in 2012, and the Ph.D. degree from the Department of Electronics and Communication Engineering, Indian Institute of Information Technology, Allahabad, India. He was an Assistant Professor with the PSIT College of Engineering, Kanpur, from 2012 to 2015. He was a Teaching Cum Research Associate (TRA) with the Department of ECE, IIIT-Allahabad, in 2020. He was an Assistant Professor (Research) with the Atria Institute of Technology, Bengaluru, from 2021 to 2023. He has been an Assistant Professor with Manipal Institute of Technology, MAHE, Manipal Campus, since 2023. He has published 24 journals and conferences (14 SCI journals and two international conferences). His research interests include wireless sensor networks, the Internet of Things, machine learning, antenna, and photonics.